The structures and Properties of Hierarchical MESOPOROUS TiO_2 Microspheres in Dye Sensitized Solar Cells Controlled by Different Reagents

Zhenquan Li[1,2], Lingdong Kong[1], Jun Liu[1,*]
[1]Department of Chemistry, Jining Medical University, Jining China
[2]School of Materials Science and Engineering, Shanghai University, Shanghai China
E-mail: lizhq18@sina.com (Z.Q. Li); conlintung@163.com (L.D. Kong); liujzh-0@163.com (J. Liu, corresponding author)

***Abstract*—In this paper, using aniline, lauryl alcohol and nonanoic acid as the structural controlling reagents, hierarchical mesoporous TiO_2 microspheres composed of connected nanoparticles are synthesized via a coupled sol-gel and solvothermal process. The dye sensitized solar cells (DSSCs) with the mesoporous TiO_2 microspheres as photoanodes demonstrate light to electricity conversion efficiency ranges from 3.9 to 6.5 %, dramatically higher than that made of P25 (3.26 %).**

Keywords- anatase TiO_2; photovoltaic efficiency; mesoporous microspheres; photoanode style

I. INTRODUCTION

Since the pioneering work of Grätzel et al in 1991 [1], dye sensitized solar cells (DSSCs) have aroused tremendous attention for their potential low costs, high efficiency and environmental benign fabrication process. Extensive investigations were performed on DSSCs and great progresses were made in this fields [2,3]. For a DSSC, the porous TiO_2 nanoparticles photoanode film is paramount in adsorbing dyes and transporting the photo-generated electrons. Under illumination, the photo-generated electrons are injected to the conduction band of TiO_2 and are further transferred across the photoanode film to the outer circuit. In order to enhance the efficiency of DSSC, different strategies were designed to improve the property of photoanode, such as increasing the specific surface areas of TiO_2 to maximize the dye molecules uptake [4,5], shortening the electron diffusion distance for the rapid transport of photo-generated electrons [6,7], post treating with TiCl4 to decrease the charge recombination or increase the light scattering [8,9], adopting sub-micron sized structures or bilayered structures to increase the light scattering effect [10-11]. In general, an ideal photoanode for DSSC should accommodate most of the beneficial characteristics such as large surface area, effective electron transport, and well light-scattering effect.

Compared with the traditional TiO_2 nanoparticles, the hierarchical mesoporous TiO_2 microspheres composed of primary nanoparticles commonly possess high specific surface area to achieve a high dye loading capacity and thus endow DSSC with high current density. Additionally, the higher light scattering effect due to the larger microspheres size elevates the light harvesting efficiency of sunlight, especially in the range of longer wavelength. Therefore, the hierarchical mesoporous TiO_2 microspheres can be regarded as preferable candidate as photoanode material. Different structural controlling reagents such as amines and alcohols were employed to assist the synthesis of hierarchical TiO_2 spheres in DSSC photoanode applications [4, 5, 10, 11]. Obviously, structural controlling reagents play important roles in controlling the assembly of primary nanocrystals toward mesoporous TiO_2 microspheres, which will further influence the conversion efficiency of DSSCs. It is imperative to understand the effect of structural controlling reagents on the structures features and photovoltaic properties of mesoporous TiO_2 microspheres.

In this paper, hierarchical mesoporous TiO_2 microspheres were synthesized using amine, alcohol and carboxylic acid as structural controlling reagents. The morphologies, surface properties and photovoltaic parameters of the materials were investigated and compared in detail. Compared with lauryl alcohol and nonanoic acid, aniline assisted the formation of mesoporous microspheres with better inter- and intra-sphere connection, highest dye adsorption capacity, as well as considerable light scatter ability, as a result, a highest conversion efficiency was achieved.

II. EXPERIMENTAL

A. Chemicals

The chemicals used in this work include tetrabutyl titanate (TBT) (Sinopharm. China), commercial P25 (Degussa), *cis*-bis (isothiocyanato)bis(2,2'-bipyridyl-4,4'-dicarboxylate)ruthenium(Ⅱ)bis-tetrabutylammonium (N719 Solaronix SA, Switzerland), Other chemicals were of reagent grade without further purification.

B. Preparation of TiO_2 mesoporous microspheres

Hierarchical mesoporous TiO_2 microspheres were synthesized via a coupled sol-gel, solvothermal and calcination process. Aniline, lauryl alcohol and nonanoic acid served as structural controlling reagents, respectively. In a typical synthesis with aniline as structural controlling reagent, 0.85 mL aniline was dissolved in 100 mL absolute ethanol, 0.55 mL KCl aqueous solution (0.073 M) was added under stirring to form a mixed solution. Then, 2.58 mL of TBT was added dropwise to the solution under violent stirring, after the appearance of white milky suspension, the mixture was kept static for 24 h. The precipitation was collected by centrifugation, washed

several times with ethanol and dried at 40 °C to afford the precursor microspheres. In the following solvothermal treatment, 0.8 g of the precursor microspheres were dispersed in 15 mL of ethanol water mixture (v:v = 2:1) by stirring, the suspension was sealed in a 25 mL Teflon-lined autoclave and heated at 160 °C for 16 h. After cooled to room temperature, the precipitation was washed with ethanol for three times and dried at 40°C to obtain mesoporous TiO_2 microspheres. The solvothermal product (0.3 g) was mixed with 0.09 g polyethylene glycol (PEG mw = 20000), suitable amount of acetic acid was added and ground for 2 h to form viscous paste, the paste was dried and calcinated at 500 °C for 30 min in air to obtain the target products (S1).

Lauryl alcohol could also assist the formation of mesoporous TiO_2 microspheres (S2), the synthesis process is the same as that for S1 except that the dosage of lauryl alcohol was 2.1 mL. When nonanoic acid was used as structure controlling reagent, microspheres (S3) was obtained, the amount of nonanoic acid was 1.25 mL, and 4 mL of water was supplemented to increase the hydrolysis, because the acidity of nonanoic acid is disadvantageous for the hydrolysis of TBT, other condition unvaried.

C. *Fabrication of DSSCs*

In the manufacture of the TiO_2 photoanode films based on the three samples, the viscous pastes of the three mesoporous TiO_2 microspheres were directly coated on fluorine-doped tin oxide conductive glasses (FTO, NSG, Japan) using a doctor-blade method with adhesive tape as frame and spacer. After dried in air, the coated FTO glass flakes were calcinated at 500 °C for 30 min to afford photoanodes. In order to improve the performance of DSSC, the photoanodes were immersed in $TiCl_4$ (0.2 M) aqueous solution and heated at 70 °C for 30 min to coat a thin layer of TiO_2 on the surface of microspheres. The treated films were scratched into 5 × 5 mm squares and calcinated again at 450 °C for 30 min. After being cooled to room temperature, the films were immersed in ethanol solution containing 0.3 mM N719 for 24 h to suck the dye. The Pt-coated FTO, formed by thermo-decomposition of H_2PtCl_6 at 380 °C for 30 min in air was used as counter electrode. The resulting sandwich-like cells were produced by the assembly of the TiO_2 photoanodes with Pt-counter electrodes. The electrolyte, composed of 0.3 M 1, 2-dimethyl-3-propyl imidazolium iodide (DMPII, Geao Co. Ltd., Wuhan), 0.5 M LiI, 0.05 M I_2, and 0.5 M 4-tert-butylpyridine in 3-methoxypropionitrile, was injected into the cells via capillarity.

D. *Characterizations*

The morphologies and structures of samples were characterized by scanning electron microscopy (SEM, JEOL JSM-6390), field emission SEM (FESEM, Hitachi S-4800), X-ray powder diffraction (XRD, Bruker D diffractometer with Cu-Kα radiation).

The specific surface areas of the samples were measured by the Brunauer-Emmett-Teller (BET) method on a Surface Area Analyzer (Micromeritics Gemini 2380) at liquid nitrogen temperature using N_2 gas as adsorbate. The samples were dried at 90 °C for 4 h and then degassed at 300 °C beforehand. The pore-size distributions were derived from the desorption branches of the isotherms using the Barrett-Joyner-Halenda (BJH) method.

The dye sensitized photoanodes were rinsed with 0.1 mol/L NaOH, and the dye adsorption capacity of photoanodes were calculated by measuring absorbances of the dye solutions on a UV-Vis spectrophotometer (TU 1900, Purkinje, China).

Photocurrent-voltage (*I-V*) measurements were performed using a Keithley 2400 sourcemeter, the light intensity of the xenon lamp solar simulator (Newport) was adjusted to 100 $mWcm^{-2}$ (AM 1.5). IPCE was measured using 7-scspec solar cell spectra test system with a 1/4 m monochromator (Saifan, China). Diffuse reflectance spectra of the photoanode TiO_2 films were also recorded on the 7-scspec spectra test system equipped with an integrating sphere (Internal DRA-2500). The film thicknesses of the photoanodes were determined on a profilometer (Dektak 150, Veeco). Electrochemical impedance spectroscopy (EIS) was recorded under open-circuit condition in the dark using a potentiostat (EG&G, M283) equipped with a frequency response detector (EG&G, FRD100). The curves were scanned in a frequency ranging from 100 kHz to 10 mHz at room temperature. The alternating voltage amplitude was set at 10 mV.

III. RESULTS AND DISCUSSION

A. *Morphological and structural characterizations*

The hierarchical mesoporous TiO_2 microspheres with different dimensions were synthesized through successive processes including hydrolysis, hydrothermal treatment and calcination. At first, amorphous precursor microspheres were synthesized by the controlled hydrolysis of TBT with the assistance of aniline, lauryl alcohol and nonanoic acid, respectively. Through the subsequent hydrothermal reaction and calcination, the amorphous spheres were converted to anatase TiO_2 with rich pores. Fig. 1a-c shows the morphologies of the porous microspheres with different dispersity after hydrothermal treatment and calcination. From the panorama shown in Fig. 1a, S1 formed with the aid of aniline contains fused microspheres with the Gaussian size distribution of 502 ± 56 nm (top left inset). FESEM of an individual sphere (top right inset) reveals that the hierarchical sphere is composed of tightly connected primary nanoparticles. The alternate light and dark regions in TEM image of an individual microsphere (down right inset) further indicates that the microspheres are porous. The morphology of S2 (Fig. 1b) includes microspheres with better dispersity than that of S1. The size of the microspheres is 522 ± 89 nm. Similar to S1, the porous microspheres are also composed of primary nanoparticles (Fig. 1b), but compared with S1, the linkage between primary nanoparticles in S2 appears more looser. S3 is also composed of porous microspheres, the size (655 ± 45 nm) of the microspheres is apparently larger than the former two samples, the monodispersity of the microspheres reveals

that the linkage among adjacent microspheres is much weaker (Fig. 1c). Because of the fusion of microspheres and the tight interconnection of primary nanoparticles, it is expected that the charge transport ability of S1 is better than S2 and S3. XRD patterns of the three products (S1-S3) are shown in Fig. 1d, the diffraction peaks of all the three products are well indexed to anatase TiO_2, showing the well crystallization of the products, which indicates the hydrothermal reaction and calcination transform the amorphous precursor to anatase TiO_2. From the full width at half-maximum of (101) facet peak, average sizes of the primary nanocrystals in the three products are calculated to be 12.1 nm (S1), 13.2 nm (S2), 14.6 nm (S3) respectively, according to Scherer equation.

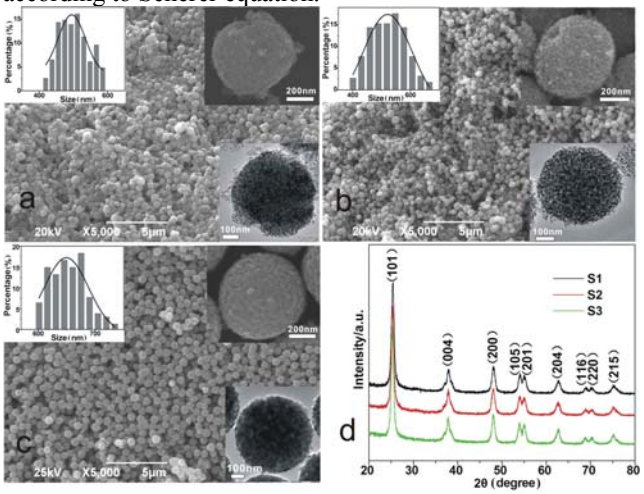

Figure 1. SEM of (a) S1, (b) S2, (c) S3 and XRD (d) of S1-S3. Inset in (a), (b), (c): top left, size distribution, top right, FESEM with higher magnificent, top down, TEM image.

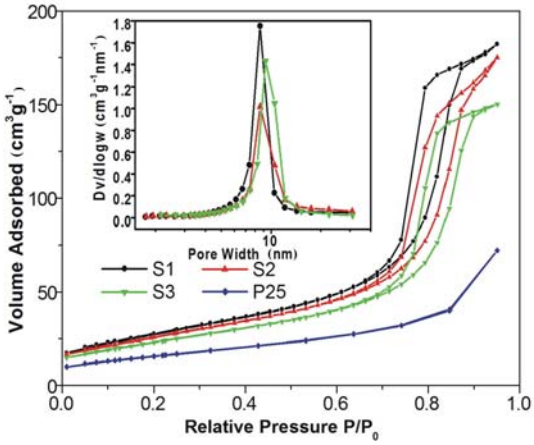

Figure 2. Nitrogen adsorption-desorption isothermal of S1-S3 and P25. Inset: BJH pore size distribution of S1-S3.

The specific surface areas and pore size distributions of S1-S3 were characterized by nitrogen gas adsorption-desorption isotherm, P25 was also measured for comparison. As shown in Fig. 2, the nitrogen absorption and desorption isotherms of S1-S3 all show type IV curves, the type H2 hysteresis loops suggest the presence of mesopores and the inkbottle-like pores shape of the as-prepared products. No hysteresis loop for P25 reveals the absence of pores. As summarized in Table 1, the specific surface areas of S1-S3 are 101, 94, 84 m^2g^{-1}, respectively. All of which are much higher than that of P25. BJH pore size distribution from the isotherms of S1-S3 shows that the average intercrystals pore sizes are 8.56, 8.59 and 9.24 nm respectively (inset), S1 displays the narrowest pore size distributions, means the more uniform pore size of S1.

TABLE I SURFACE PROPERTIES OF S1-S3 AND P25.

Sample name	S1	S2	S3	P25
BET specific surface area (m^2g^{-1})	101.01	94.74	84.16	57.20
Pore size(nm)	8.56	8.59	9.24	
Pore volume (cm^3g^{-1})	0.2836	0.2638	0.2370	

B. Optical and photoelectrochemical properties

In order to investigate the application of the three mesoporous microspheres products (S1-S3) in photoanodes of DSSC, photoanode films made of S1-S3 with the thickness of about 13 μm were spread onto FTO using a doctor blade method followed by $TiCl_4$ treatment and calcination. P25 photoanode film with the similar thickness was also fabricated for comparison. The dye adsorption capacity of the photoanodes films made of S1-S3 and P25 were calculated by measuring the concentration of dye solutions rinsed from the sensitized photoanodes. The dye adsorption capacity of P25 photoanode is 0.89×10^{-7} $molcm^{-2}$. While for photoanodes of S1-S3, the values are 1.81×10^{-7}, 1.33×10^{-7}, and 1.14×10^{-7} $molcm^{-2}$, respectively, dramatically higher than P25 (Table 2). The photoanode made of S1 demonstrates the highest dye adsorption capacity, implies the highest light harvesting ability and further the highest photocurrent density (J_{sc}).

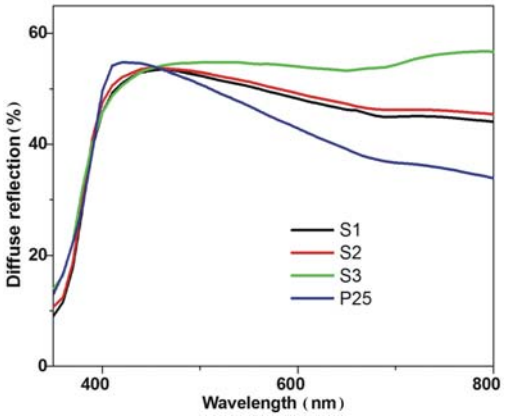

Figure 3. Diffuse reflection spectra of photoanodes made of S1-S3 and P25

Since N719 dye has low absorbance at longer wavelength, the increase in light scattering effect of photoanode film can enhance the light harvesting ability and further the conversion efficiency of DSSC. Light scattering effect of photoanode can be quantified by diffusion reflection spectroscopy. From Fig. 3, photoanode films made of S1-S3 and P25 all demonstrate high diffuse

reflection intensity in the region of 400-450 nm, the diffuse reflection ability of P25 photoanode is the highest in this region, while decreases sharply at longer wavelength (450-800 nm) for the small particles size. The diffuse reflection intensities of S1-S3 are much higher in this region, reveals that sub-micron grade spheres possess higher light scattering ability. The diffuse reflection intensity of S3 even increases at longer wavelength because of the apparently larger microsphere diameter. It is evident that the light harvesting ability of N719 in this region can be enhanced.

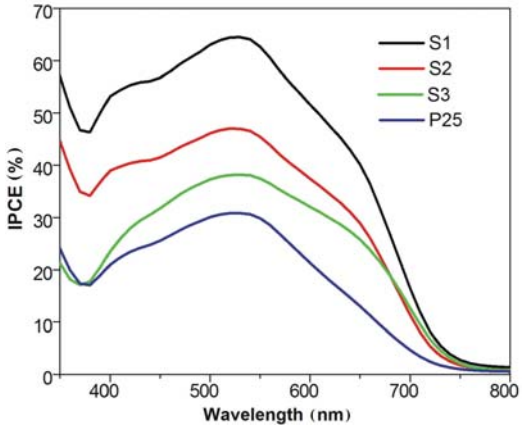

Figure 4. IPCE of DSSCs based on S1-S3 and P25.

Because of the higher dye adsorption capacity and the well light scattering effect, the photoanodes made of S1-S3 should give rise to higher photovoltaic efficiency. The photovoltaic response of the DSSCs based on S1-S3 and P25 were compared by IPCE. It is known that IPCE is determined by the light absorption efficiency of dye, the electron injection efficiency and collecting efficiency of the injected electron at conducting glass substrate, which strongly depend on the morphology and surface properties of the photoanode film materials. As shown in Fig. 4, the photoanode films made of S1-S3 showed higher IPCE values than that of P25 from 350 to 750 nm with the similar thickness. The higher IPCE of S1-S3 photoanode than P25 photoanode at the range of 350-600 nm mainly ascribed to the higher dye loading capacities derived from the high specific surface areas. Moreover, in the wavelength range over 600 nm, the absorbance of N719 is weak, the side peak at 600-750 nm for S1-S3 films indicates that the enhancement in IPCE value is originated from the elevated light scattering effect, which improved the light harvesting of dye in this region. The side peak for S3 is more apparent than that of S1 and S2, which agrees with the diffusion reflection spectra, showing the light scatter effect is another factor relevant to the IPCE values. As for the photoanodes of S1-S3, the IPCE value of S1 is the highest, indicating that although light scattering effect is important in elevating the light harvesting efficiency, the contribution of dye loading capacity to IPCE is dominant.

Photo-generated electrons collection efficiency is also crucial to IPCE and conversion efficiency of DSSC. The photo-generated electrons should be transferred across the photoanode film to outer circuit before being recombined by I_3^- at TiO_2/electrolyte interface, so that higher electron collection efficiency can be obtained. EIS was used to investigate the recombination lifetime of the photo-generated electrons during the transferring across TiO_2 film. Fig. 5 shows the Bode mode of EIS plots of DSSCs based on S1-S3 and P25 nanoparticles. Generally, in Bode mode of EIS plots of DSSC, the three characteristic peaks from high to low frequency are respectively related to the charge transfer in the counter electrode, electron diffusion and recombination in photoanode and the Nernstian diffusion in electrolyte [12]. The electron recombination lifetime (τ_e) during the transfer across photoanode film can be calculated from the maximum frequency (f_{max}) of the peak at intermediate frequency as: $\tau_e = 1/2\pi f_{max}$ [13]. According to the equation, lower frequency of the middle peak means the longer recombination lifetime, which permits longer electron diffusion distance before recombination. As a result, the photocurrent density will be increased. From Fig. 5, τ_e values are 34.1, 19.8, 13, and 4.2 ms for S1, S2, S3 and P25, respectively. The much longer electron recombination lifetime of S1-S3 reveals the effective delay in recombination of the injected electron by I_3^- during the transfer process across photoanode films. This may be ascribed to the more tightly attachments of primary particles in the mesoporous microspheres than that between P25 nanoparticles. As for DSSCs with mesoporous TiO_2 microspheres as photoanode materials, DSSC based on S1 shows the dramatically longer electrons recombination lifetime than that of S2 and S3. This can be attributed to the better inter- and intra- spheres connection, as well as the partial oriented attachment of adjacent primary nanocrystals in S1, which lead to the higher charge collection efficiency and further contribute to higher IPCE and J_{sc}.

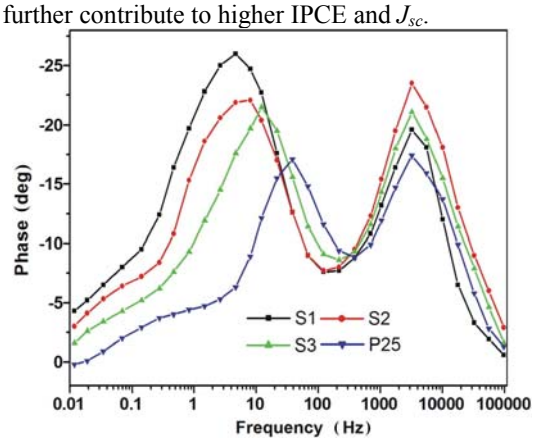

Figure 5. Bode mode of EIS of DSSCs based on S1-S3 and P25 in the dark under open-circuit condition.

C. *Photovoltaic properties*

To investigate the effect of structural controlling reagents on the photovoltaic efficiency of the mesoporous microspheres, DSSC based on S1-S3 and P25 were characterized by measuring the current-voltage behavior under AM 1.5 illumination. Fig. 6 shows the typical *I-V* curves of cells based on S1-S3 and P25, the resultant photovoltaic parameters were summarized in Table 2. The

approximately 13 μm thick photoanode film made of P25 shows J_{sc} of 7.09 mAcm^{-2}, V_{oc} of 0.82 V, and over-all energy conversion efficiency (η) of 3.26 %. Compared with DSSC based on P25, J_{sc} and η of the cells based on S1-S3 are enhanced to different degrees, while V_{oc} only shows slight decrease, which indicates the mesoporous TiO_2 microsphere is more suitable as photoanode materials. This is attributed to the higher dye adsorption capacity and the light scattering capability, as well as the longer electrons recombination lifetime of mesoporous TiO_2 microspheres. As for the DSSCs based on mesoporous TiO_2 microspheres, J_{sc} and η of the cell based on S1 are 15.24 mAcm^{-2} and 6.55 %, respectively, which are dramatically higher than that of S2 and S3, indicating the structural controlling reagents significantly affect η of photoanode materials. Superior to lauryl alcohol and nonanoic acid, aniline assist the formation of mesoporous TiO_2 microspheres with better inter- and intra-spheres connection, higher dye adsorption capacity and acceptable light scattering capability. All these factors contribute to the better photovoltaic efficiency of DSSC. Herein, it should be pointed out that, the fill factor of the cells based on S1-S3 are not ideal, restricting the overall conversion efficiency of the cells, this maybe related to the electrolyte or other factors of the cells. Further optimizing experiments are currently performed to overcome this deficiency.

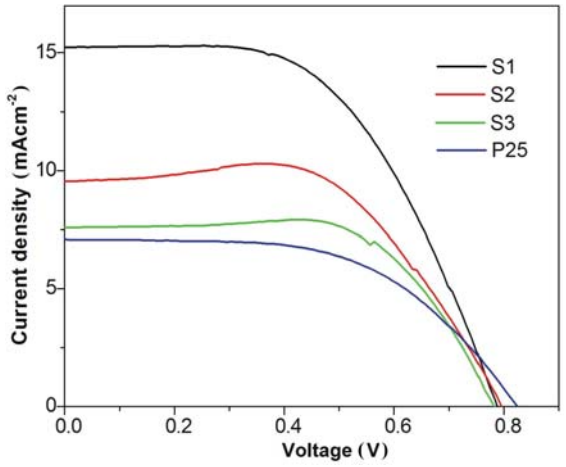

Figure 6. I-V curve of DSSCs based on S1-S3 and P25.

TABLE II PHOTOVOLTAIC PROPERTIES OF THE DSSCS BASED ON S1-S3 AND P25.

Sample name	thickness (μm)	V_{oc} (V)	J_{sc} (mAcm^{-2})	*FF*	η (%)	Adsorbed dye(molcm^{-2})
S1	13.4	0.79	15.24	0.55	6.55	1.81×10^{-7}
S2	13.1	0.80	9.55	0.61	4.64	1.33×10^{-7}
S3	13.1	0.78	7.59	0.66	3.89	1.14×10^{-7}
P25	13.5	0.82	7.09	0.56	3.26	0.89×10^{-7}

IV. CONCLUSIONS

In conclusion, hierarchical mesoporous TiO_2 microspheres were synthesized with the assistance of different type of structure controlling reagents. Due to the higher dye adsorption capacity, acceptable light scattering capability and the better inter- and intra-spheres connection, mesoporous microspheres assisted by aniline, used as a photoanode, present DSSC with dramatically higher conversion efficiency.

ACKNOWLEDGMENT

This work was financially supported by Jining Science and Technology Bureau (No.2011041) and the Shandong Province Colleges and Universities Outstanding Young Teachers in Domestic Visiting Scholars Project.

REFERENCES

[1] O'Regan B, Grätzel M., "A low-cost, high-efficiency solar cell based on dye-sensitized colloidal TiO_2 films," Nature, vol. 353, pp. 737–740, October 1991.

[2] Grätzel M., "Conversion of sunlight to electric power by nanocrystalline dye-sensitized solar cells," J Photochem. Photobiol. A, vol. 164, pp.3–14, June 2004..

[3] Grätzel M., "Mesoscopic solar cells for electricity and hydrogen production from sunlight," Chem. Lett., vol. 34, pp. 8–13. January 2005.

[4] Yang W.G., Wan F.R., Chen Q.W., "Controlling synthesis of well-crystallized mesoporous TiO_2 microspheres with ultrahigh surface area for high-performance dye-sensitized solar cells," J Mater. Chem., vol. 20, pp.2870–2876, April 2010.

[5] Shao W., Gu F., Li C.Z., Lu M.K., "Interfacial confined formation of mesoporous spherical TiO_2 nanostructures with improved photoelectric conversion efficiency," Inorg. Chem., vol. 49, pp. 5453–5459, June 2010.

[6] Chen Q.W., Xu D.S., "Large-scale, noncurling and free-standing crystallized TiO_2 nanotube arrays for dye-sensitized solar cells," J Phys. Chem. C, vol. 113, pp. 6310–6314, April 2009.

[7] Kang T.S., Smith A.P., Taylor B.E., Durstock M.F., "Fabrication of highly-ordered TiO_2 nanotube arrays and their use in dye-sensitized solar cells," Nano. Lett., vol. 9, pp. 601–606, February 2009.

[8] Park N.G., Schlichthörl G., Van de Lagemaat J., "Dye-sensitized TiO_2 solar cells: Structural and photoelectrochemical characterization of nanocrystalline electrodes formed from the hydrolysis of $TiCl_4$," J Phys. Chem. B, vol. 103, pp. 3308–3314, April 1999.

[9] Sommeling PM., O'Regan BC., Haswell RR., Smit HJP., "Influence of a $TiCl_4$ post-treatment on nanocrystalline TiO_2 films in dye-sensitized solar cells," J Phys. Chem. B, vol. 110, pp. 19191–19197, October 2006.

[10] Koo H.J., Kim Y.J., Lee Y.H., "Nano-embossed hollow spherical TiO_2 as bifunctional material for high-efficiency dye-sensitized solar cells." Adv. Mater., vol. 20, pp. 195–199, January 2008.

[11] Chen D.H., Huang F.Z., Cheng Y.B., "Mesoporous anatase TiO_2 beads with high surface areas and controllable pore sizes: A superior candidate for high-performance dye-sensitized solar cells," Adv. Mater., vol. 21, pp. 2206–2210, May 2009.

[12] Wang Q., Moser JE., Grätzel M., "Electrochemical impedance spectroscopic analysis of dye-sensitized solar cells," J Phys. Chem. B, vol. 109, pp. 14945–14953, August 2005.

[13] Kern R., Sastrawan R., Ferber J., "Modeling and interpretation of electrical impedance spectra of dye solar cells operated under open-circuit conditions," Electrochim. Acta. vol. 47, pp. 4213–4225, October 2002.